JOURNAL OF SYNCHROTRON RADIATION

ISSN 1600-5775

Received 5 January 2017
Accepted 8 June 2017

Edited by Y. Amemiya, University of Tokyo, Japan

Keywords: multilayer; X-ray; interface; thermal conductivity.

Temperature-dependent thermal properties of Ru/C multilayers

Shuai Yan, Hui Jiang,* Hua Wang, Yan He, Aiguo Li, Yi Zheng, Zhaohui Dong and Naxi Tian

Shanghai Synchrotron Radiation Facility, Shanghai Institute of Applied Physics, Chinese Academy of Sciences, Zhangheng Road 239, Pudong District, Shanghai 201204, People's Republic of China.
*Correspondence e-mail: jianghui@sinap.ac.cn

Multilayers made of Ru/C are the most promising candidates when working in the energy region 8–20 keV. The stability of its thermal properties, including thermal expansion and thermal conduction, needs to be considered for monochromator or focusing components. Ru/C multilayers with periodic thicknesses of 3, 4 and 5 nm were investigated *in situ* by grazing-incidence X-ray reflectometry and diffuse scattering in order to study their thermal expansion characteristics as a function of annealing temperature up to 400°C. The thermal conductivity of multilayers with the same structure was also measured by the transient hot-wire method and compared with bulk values.

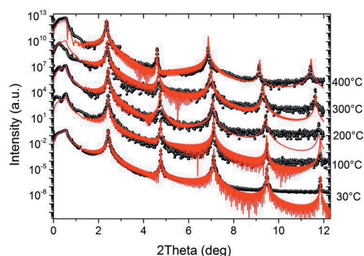

© 2017 International Union of Crystallography

1. Introduction

Ru/C (Stampanoni *et al.*, 2006; Störmer *et al.*, 2016) and Ru/B_4C multilayers (Sawhney *et al.*, 2011) are widely used in the energy range 8–20 keV due to their high-reflectance performance and stable interfacial structure. With the development of third-generation synchrotron radiation and free-electron laser facilities, reflective multilayers are required to treat higher thermal loads to realise the high-throughput experimental mode. In a monochromator, the first multilayer absorbs most of the incident white-beam flux, normally with a power density far exceeding several watts per square millimeter, which produces a thermal bump, leading to wavefront errors (Rutishauser *et al.*, 2013). Once the cooling system fails to work, the multilayer can rapidly reach high temperatures (Ziegler *et al.*, 1989). Heat-load-induced deformation and thermal stress due to mismatch of the thermal expansion coefficient between multilayers and substrate have been investigated in recent years (Cheng *et al.*, 2014, 2015). In addition, for coatings on focusing components such as Kirkpatrick–Baez mirrors (Yumoto *et al.*, 2013) or multilayer Laue lenses (Kang *et al.*, 2006) without cooling, heat may accumulate on the coating surface due to pink-beam incidence and/or the influence of heating the sample when the focal length is small. Based on the above-mentioned situations, measurements of thermal expansion and thermal transport become important for modelling thermal distribution and estimating stability in multilayers. Scientists from ESRF have optimized (Zhang *et al.*, 2013), simulated (Sawhney *et al.*, 2011) and measured (Rutishauser *et al.*, 2013) multilayers in order to minimize such potential damage.

Besides thermal expansion, thermal conductivity of the multilayers is the other important factor, and decides the heat exchange rate with the environment and the equilibrium

temperature of the multilayers. Due to the nanometer scale of the layer thickness in the multilayer, the thermal conductivity of the multilayer may be different from the material bulk values. Some effective methods have been used to measure the in-plane (parallel to the interfaces) or cross-plane (perpendicular to the interfaces) thermal conductivity of thin-film structures, including the transient hot-strip technique (Belkerk *et al.*, 2012), the 3-ω technique (Chen, 1997), photothermal deflection spectroscopy (Moorhead *et al.*, 2010) and micro-Raman spectroscopy (Luo *et al.*, 2014), *etc*.

Some related studies presented the influence of crystallites in Ru/C or Ru/B_4C multilayers. Ruthenium layers were found to form hexagonal ruthenium crystallites after annealing which enhanced the uncorrelated roughness (Nguyen *et al.*, 1992). A sputtering atmosphere with different oxygen fractions was proved to clearly influence crystallites of Ru and their reflectivity (Walton & Kortright, 1995). Our previous study determined the structural stability of Ru/C multilayers during low-temperature treatment (Jiang *et al.*, 2015).

In this paper, *in situ* measurements at different annealing temperatures including grazing-incidence X-ray reflectometry and rocking-curve scattering were used to investigate the structure evolution of Ru/C multilayers, and temperature-dependent cross-plane thermal conductivities along the multilayer depth were measured based on the transient hot-wire method.

2. Experiments and methods

Six pieces of Ru/C multilayer samples (S1–S6) were deposited by direct current magnetron sputtering on silicon (110) wafers of size 35 mm × 22.5 mm and thickness 0.75 mm at room temperature by Incoatec GmbH, Germany. The thickness ratio Γ and the period number N for all samples were 0.5 and 100, respectively. The design periodic thicknesses for these samples were 3 nm (S1 and S2), 4 nm (S3 and S4) and 5 nm (S5 and S6). Each pair of samples with the same structure were deposited simultaneously.

Samples (S1, S3 and S5) were measured by grazing-incidence X-ray reflectometry (XRR) and diffuse scattering (XDS) at the X-ray diffraction beamline (BL14B1) of Shanghai Synchrotron Radiation Facility. An X-ray energy of 10 keV was selected using a silicon double-crystal monochromator with energy resolution of $\sim 1.5 \times 10^{-4}$; the beam size before the samples was ~0.4 mm × 0.4 mm. The grazing-incidence measurement were made by θ–2θ scan. The diffuse scattering measurements were made by rocking-curve scan by fixing the point detector and scanning the incidence angle near the first Bragg reflections. During the measurements, the multilayers were placed in a chamber and the wafers were heated up from room temperature up to ~400°C in an air atmosphere. Theoretical XRR curves as a function of grazing-incidence angle can be calculated based on Parratt's recurrence formula (Parratt, 1954). The interfacial widths from layer to layer satisfy the law of the structure growth $\sigma_j^2 = \sigma_{j-1}^2 + hD$ (Pleshanov, 2004), where σ_j is the interfacial width at the jth interface from the substrate, D is the periodic thickness and parameter h is the roughness growth rate. The experimental reflectivity data were fitted based on theoretical data based on the method of least squares.

The cross-plane thermal conductivity φ of the multilayers (S2, S4 and S6) and silicon wafer were measured by the transient hot-wire method (Healy *et al.*, 1976) at −30, 40 and 117°C, respectively. During the measurements, each sample was divided into two parts and a thin nickel wire was clamped on the multilayer surfaces as a sensor. The temperature of the wire was recorded while applying a transient voltage of 2.5 V for a short duration. Regarding the multilayers as a whole, the working equation satisfies Fourier's law. While the radius of the wire is small, the working equation can be deduced to be

$$\delta T = \frac{q}{4\pi\varphi}\ln(t) + \frac{q}{4\pi\varphi}\ln\left[\frac{4\alpha}{r_o^2\exp(\gamma)}\right],$$

where δT is the temperature deviation of the wire at time t, q = 8.733 W is the applied power for unit hot wire, α is the thermal diffusivity and $\gamma \simeq 0.577$ is Euler's constant (Healy *et al.*, 1976).

3. Results and discussions

The Ru/C multilayers S1, S3 and S5 were measured by using grazing-incidence reflectometry at room temperature, 100, 200, 300 and 400°C. The reflectivity curves and their fitting curves are shown in Fig. 1. The periodic thicknesses were calculated using the modified Bragg equation accurately and the structural parameters were obtained by curve-fitting based on a reasonable initial structure including the structure growth model, as can be seen in Table 1, where the density of Ru and C are 12.2 g cm^{-3} (Ru crystal) and 2.22 g cm^{-3} (graphite), respectively. Because the sample chamber was not filled with protective gas during the measurement, surface oxidation also needs to be considered in the fitting model. The results show that thinner multilayers S1 and S3 were easily oxidized at the surface when the sample temperature reached 300°C. The thermal expansion of periodic thickness D gradually increased as a function of annealing temperature. The thinner sample has a larger coefficient of thermal expansion. The fitting results found in Fig. 2 show different tendencies of thickness change for the two materials in different samples. The thickness change of each layer comes from two effects: thermal expansion itself and the thermal-induced interdiffusions between two adjacent layers. In S1, since the layer thickness is small, interdiffusion played a dominate role. The Ru/C interfaces moved towards the ruthenium layers due to interdiffusion, which resulted in the thicknesses and densities of the carbon layers increasing simultaneously and significantly. With the increasing of layer thickness, the influence from the material itself gradually became dominant. While the periodic thickness reaches 5 nm, the ruthenium layers were found to be obviously crystalline (Jiang *et al.*, 2015) and their densities decreased. The thicknesses of the carbon layer showed little changes in our annealing experiment at temperatures below 400°C (Tu *et al.*, 2014), which meant that the interdiffusion behavior was blocked to some extent and became weak. The

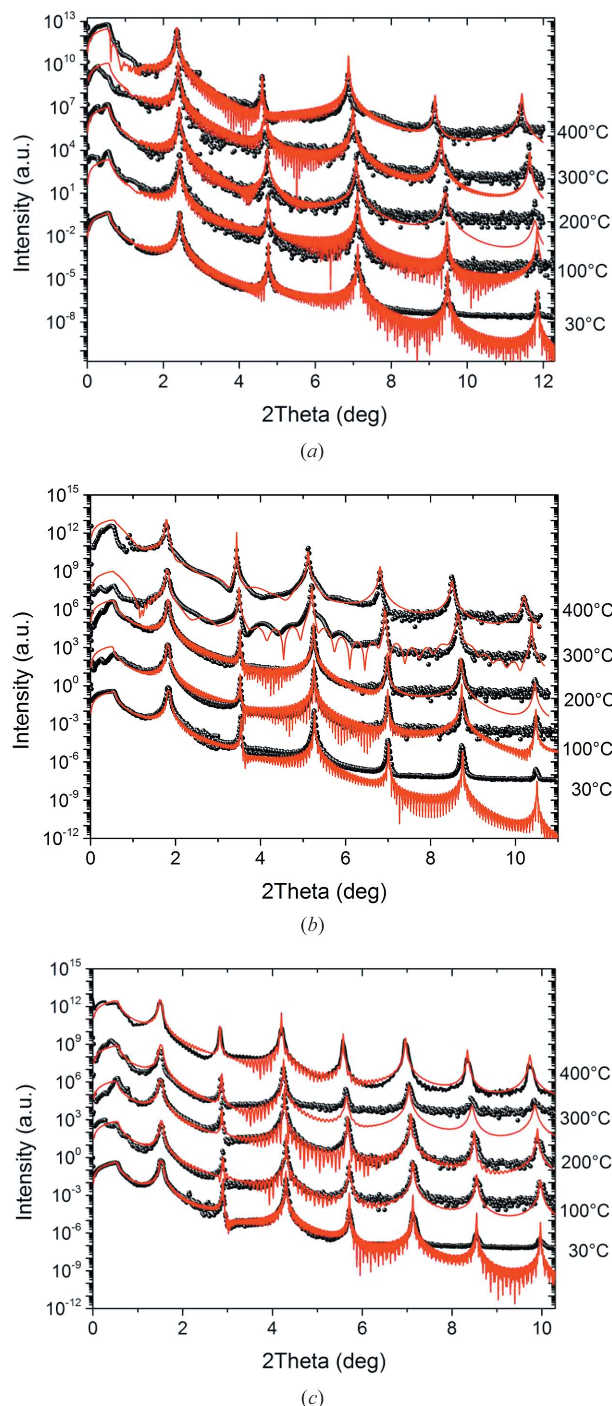

Figure 1
Grazing-incidence reflectivity curves (dots) for S1 (*a*), S3 (*b*) and S5 (*c*), measured when the samples were annealed at room temperature, 100, 200, 300 and 400°C, and their fitting curves (lines).

thickness change of the multilayer was mainly from the expansion of the ruthenium layers.

The law of the structure growth was introduced to the multilayer model. The roughness growth rate, which is the rate of change of roughness as a function of period number, revealed a correlation of interfacial roughnesses sensitively with a change of periodic thickness and annealing temperature. Before the multilayers were annealed, the roughness

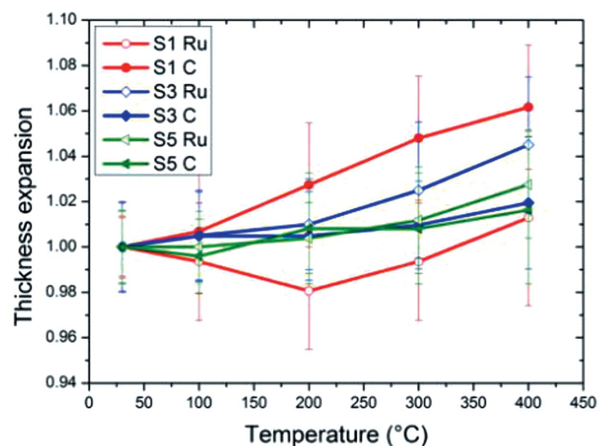

Figure 2
Thermal expansion of Ru and C layers in multilayers S1 (circle), S3 (square) and S5 (triangle) with increasing annealing temperature.

growth rates of the two materials were similar and became larger with increasing periodic thickness. As the annealing temperature increased, the roughness growth rates increased significantly. Comparing the three samples, the situations were still different. In S1, the roughness growth rates changes were small compared with the other two samples and relatively similar for the two materials. This was because the interdiffusion, which plays a dominant role in thermal expansion, was relatively symmetric in the Ru-on-C and C-on-Ru interfaces and was not obviously influenced by the increasing period number. With the increases of the periodic thicknesses in S3 and S5, the roughness growth rate in the Ru-on-C interfaces clearly increased more than in the C-on-Ru interfaces as a function of temperature. Referring the fitting results of the thickness and density, this phenomenon can be interpreted as the gradually crystallized Ru layers having larger surface free energy and fewer void streaks in their structures so that the upper C layers more easily form smooth layers rather than diffuse into Ru layers or island growth (Mo *et al.*, 1990; Lüth, 2010).

The rocking-curve diffuse scattering curves measured near the first Bragg reflection for three samples can be seen in Fig. 3.

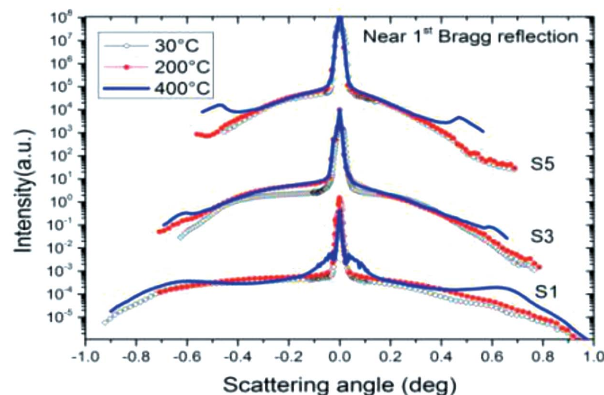

Figure 3
Rocking-curve diffuse scattering curves near the first Bragg reflection for multilayers S1, S3 and S5 measured at room temperature, 200 and 400°C.

Table 1
Structural parameters for S1, S3 and S5 by fitting the grazing-incidence reflectivity curves at room temperature, 100, 200, 300 and 400°C.

	Temperature (°C)	Periodic thickness (nm)		Thickness (nm)	Density (%)	Interfacial width at the bottom layer (nm)	Roughness growth rate ($\times10^{-4}$)
S1	30	3.001 ± 0.001	Ru	1.55 ± 0.01	90.75 ± 7.19	0.27 ± 0.07	0.33 ± 0.03
			C	1.46 ± 0.01	99.89 ± 3.10	0.28 ± 0.05	0.32 ± 0.05
	100	3.006 ± 0.001	Ru	1.54 ± 0.02	99.61 ± 5.21	0.23 ± 0.04	1.66 ± 0.06
			C	1.47 ± 0.02	134.42 ± 5.32	0.28 ± 0.05	0.67 ± 0.04
	200	3.025 ± 0.002	Ru	1.52 ± 0.02	96.86 ± 3.36	0.25 ± 0.05	1.65 ± 0.04
			C	1.50 ± 0.02	109.33 ± 4.27	0.24 ± 0.04	2.61 ± 0.08
	300	3.063 ± 0.002	Ru	1.54 ± 0.02	90.26 ± 4.33	0.31 ± 0.08	1.72 ± 0.08
			C	1.53 ± 0.02	128.27 ± 4.01	0.24 ± 0.07	2.94 ± 0.09
	400	3.123 ± 0.003	Ru	1.57 ± 0.03	99.96 ± 3.56	0.25 ± 0.07	2.24 ± 0.12
		(oxidation of 3 periods)		(1.71 ± 0.09)	(78.28 ± 3.14)		
			C	1.55 ± 0.02	130.77 ± 4.94	0.27 ± 0.08	2.56 ± 0.16
				(1.70 ± 0.11)	(94.99 ± 6.07)		
S3	30	4.061 ± 0.008	Ru	2.00 ± 0.02	92.97 ± 3.17	0.28 ± 0.04	0.25 ± 0.04
			C	2.06 ± 0.02	99.91 ± 4.01	0.29 ± 0.03	0.53 ± 0.06
	100	4.068 ± 0.008	Ru	2.01 ± 0.02	93.66 ± 4.13	0.27 ± 0.05	1.23 ± 0.05
			C	2.07 ± 0.02	100.67 ± 4.52	0.25 ± 0.05	1.72 ± 0.09
	200	4.081 ± 0.002	Ru	2.02 ± 0.02	89.63 ± 3.44	0.30 ± 0.04	1.68 ± 0.04
			C	2.07 ± 0.02	117.19 ± 4.37	0.25 ± 0.06	3.43 ± 0.11
	300	4.125 ± 0.001	Ru	2.05 ± 0.03	92.27 ± 6.04	0.28 ± 0.07	1.45 ± 0.15
		(oxidation of 2 periods)		(2.23 ± 0.09)	(107.97 ± 6.54)		
			C	2.08 ± 0.02	73.74 ± 4.98	0.24 ± 0.07	6.03 ± 0.20
				(2.16 ± 0.08)	(115.71 ± 5.23)		
	400	4.192 ± 0.004	Ru	2.09 ± 0.03	95.55 ± 4.78	0.24 ± 0.08	1.43 ± 0.14
		(oxidation of 2 periods)			(109.95 ± 5.97)		
			C	2.10 ± 0.03	71.05 ± 5.09	0.27 ± 0.08	6.92 ± 0.19
					(70.01 ± 5.77)		
S5	30	5.025 ± 0.005	Ru	2.55 ± 0.02	86.17 ± 3.49	0.17 ± 0.05	1.31 ± 0.06
			C	2.46 ± 0.02	98.45 ± 4.21	0.25 ± 0.05	1.35 ± 0.04
	100	5.019 ± 0.005	Ru	2.55 ± 0.02	85.24 ± 3.87	0.16 ± 0.06	1.79 ± 0.08
			C	2.45 ± 0.02	128.75 ± 4.53	0.28 ± 0.05	3.59 ± 0.06
	200	5.044 ± 0.003	Ru	2.56 ± 0.02	85.45 ± 4.04	0.16 ± 0.05	1.99 ± 0.07
			C	2.48 ± 0.03	100.01 ± 4.36	0.22 ± 0.06	4.01 ± 0.14
	300	5.073 ± 0.010	Ru	2.58 ± 0.03	87.04 ± 4.25	0.16 ± 0.06	3.29 ± 0.09
			C	2.48 ± 0.03	97.59 ± 4.79	0.25 ± 0.07	7.34 ± 0.17
	400	5.141 ± 0.010	Ru	2.62 ± 0.03	89.20 ± 5.03	0.16 ± 0.08	3.69 ± 0.16
			C	2.50 ± 0.04	108.73 ± 5.19	0.26 ± 0.06	10.70 ± 0.24

The XDS measurement distinguished between the roughness and the interdiffusion signals. The results revealed that the main part of the roughness increase was in the high-frequency region. When the annealing temperature reached 400°C, the Yoneda wings on both sides in the high-frequency region can be measured clearly. High-frequency roughness is known to be more difficult to replicate with the layer deposition compared with low-frequency roughness (Stearns, 1992) so that the vertical correlation in the Ru/C multilayer decays after annealing. In the low-frequency region near the Bragg peak, the roughness increased more obviously with increasing temperature in thinner multilayers. This reveals a better vertical correlation in thinner multilayers which matches the smaller roughness growth rate determined by XRR.

Multilayers S2, S4 and S6 and an uncoated silicon wafer (the same as the wafers used for the multilayer coating) were used to measure the cross-plane thermal conductivity by the transient hot-wire method. Each curve of the temperature deviation *versus* the natural logarithm of increasing test time showed two inflection points, at $t = 10^{-4}$ s and $t = 10^{-2}$ s. These curves can be linear fitted into three segments based on these inflection points, as can be seen in Fig. 4. There is no obvious regularity of the slopes of the first fitting curves, not only for different temperatures but also for different samples. The slopes of the third fitting curves are similar and close to the slope of the fitting curve in the uncoated silicon wafer. Considering the structure of the multilayers, the three

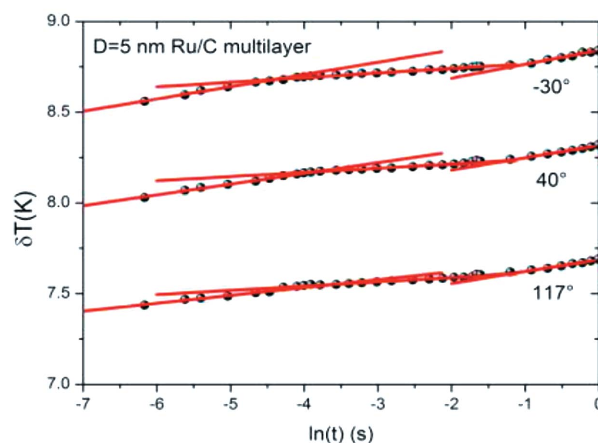

Figure 4
Temperature deviations of the wire with increasing natural logarithm of test time for S6 at different initial temperatures (dots) and piecewise linear fittings (lines).

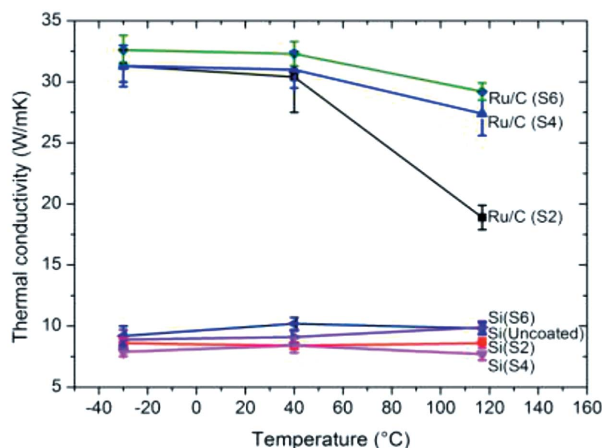

Figure 5
Thermal conductivities of Ru/C multilayers (S2, S4 and S6) and silicon wafers (S2, S4, S6 and uncoated).

segments of the fitting curves correspond to surface contamination and/or oxidation, the multilayer coating and the silicon substrate. The thermal conductivities of the multilayer structures and silicon substrates at different temperatures can be easily deduced by fitting the second- and third-segment curves, as can be seen in Fig. 5. Each layer thickness in the multilayer structure is sufficiently small that it cannot be distinguished independently. The results reveal that the thermal conductivities of multilayers increased with increasing periodic thickness and decreased with increasing test temperature. The thermal conductivities, $\sim 30\ \mathrm{W\,mK^{-1}}$, were less than the values of bulk ruthenium [$\sim 116\ \mathrm{W\,mK^{-1}}$ (http://www.azom.com/article.aspx?ArticleID=9275)] and polycrystalline graphitic carbon [$\sim 80\ \mathrm{W\,mK^{-1}}$ (https://www.netzsch-thermal-analysis.com/en/materials-applications/polymers/polycrystalline-graphite-thermal-conductivity)], but higher than previous reports on amorphous carbon thin films ($\sim 1\ \mathrm{W\,mK^{-1}}$) (Bullen *et al.*, 2000). Thermal conductivity reduction may result from the size and interface effects for ultra-thin films, which is normally predicted by the semi-classical Boltzmann transport equation (Chen, 1997; Feng *et al.*, 2009; Lambropoulos *et al.*, 1989). Regarding the entire multilayer as a composite thin film, since the entire thickness is generally larger than the phonon mean free path l of materials (normally several angstroms to several hundred nanometers) and the time scale of interest was much larger than the relaxation time for phonons, the heat diffusion model can still be considered valid (Belkerk *et al.*, 2012). If using a simplified model of effective thermal conductivity (Moorhead *et al.*, 2010),

$$ND/\varphi = \sum_i d_i/\varphi_i,$$

where d_i is the ith layer thickness, the thermal conductivity of each layer can be estimated within the range from $\sim 17\ \mathrm{W\,mK^{-1}}$ to the bulk value. Based on an effective model deduced from the Boltzmann transport equation by Alvarez & Jou (2007),

$$\varphi = \frac{\varphi_{\rm bulk}(ND)^2}{2\pi^2 l^2}\left\{\left[1+4\left(\frac{\pi l}{ND}\right)^2\right]^{1/2}-1\right\},$$

the calculated thermal conductivity is found to be very close to our measured results when the phonon mean free path l is about several tens of nanometers.

4. Conclusion

The thermal expansion and cross-plane thermal conductivity of Ru/C multilayers with different periodic thicknesses were measured by *in situ* grazing-incidence X-ray reflectometry and the transient hot-wire method. The interfacial roughness evolution with period number was determined by fitting XRR curves. By combining X-ray diffuse scattering, the interfacial roughness and interdiffusion were found to be strongly related to the thickness of the ruthenium layer and its crystallinity at different annealing temperatures. The thermal conductivity reductions of Ru/C multilayers were found compared to both the values of bulk materials. The phonon mean free path is estimated based on Alvarez's model. These studies are useful for estimating the thermal distribution and thermal stability for multilayer monochromators and other multilayer optics without cooling systems.

Acknowledgements

Incoatec GmbH is thanked for the fabrication of Ru/C multilayers. The authors would like to thank their colleagues from the SSRF: Drs Bin Zhao and Xingmin Zhang for experimental support in BL14B1 grazing-incidence reflectometry, scattering and high-angle diffraction measurements, and Dr Xiaolong Li for the *in situ* heating setup. Xi'an Xiaxi Electronic Technology Co. Ltd is thanked for the measurement of thermal conductivity using the TC3000 thermal conductivity meter. This work was supported by the National Natural Science Foundation of China (see below for details) and the Knowledge Innovation Program of Chinese Academy of Sciences.

Funding information

The following funding is acknowledged: National Natural Science Foundation of China (award No. 11304339; award No. U1432244; award No. U1332120; award No. 11205235).

References

Alvarez, F. X. & Jou, D. (2007). *Appl. Phys. Lett.* **90**, 083109.
Belkerk, B. E., Soussou, M. A., Carette, M., Djouadi, M. A. & Scudeller, Y. (2012). *J. Phys. D*, **45**, 295303.
Bullen, A. J., O'Hara, K. E., Cahill, D. G., Monteiro, O. & von Keudell, A. (2000). *J. Appl. Phys.* **88**, 6317–6320.
Chen, G. (1997). *J. Heat Transfer*, **119**, 220–229.
Cheng, X., Morawe, C., Peffen, J. & Zhang, L. (2014). *Proc. SPIE*, **9207**, 920709.
Cheng, X., Zhang, L., Morawe, C. & Sanchez del Rio, M. (2015). *J. Synchrotron Rad.* **22**, 317–327.
Feng, B., Li, Z. & Zhang, X. (2009). *Thin Solid Films*, **517**, 2803–2807.

Healy, J. J., de Groot, J. J. & Kestin, J. (1976). *Physica B+C*, **82**, 392–408.

Jiang, H., He, Y., He, Y., Li, A., Wang, H., Zheng, Y. & Dong, Z. (2015). *J. Synchrotron Rad.* **22**, 1379–1385.

Kang, H. C., Maser, J., Stephenson, G. B., Liu, C., Conley, R., Macrander, A. T. & Vogt, S. (2006). *Phys. Rev. Lett.* **96**, 127401.

Lambropoulos, J. C., Jolly, M. R., Amsden, C. A., Gilman, S. E., Sinicropi, M. J., Diakomihalis, D. & Jacobs, S. D. (1989). *J. Appl. Phys.* **66**, 4230–4242.

Luo, Z., Liu, H., Spann, B. T., Feng, Y., Ye, P., Chen, Y. P. & Xu, X. (2014). *Nanoscale Microscale Thermophys. Eng.* **18**, 183–193.

Lüth, H. (2010). *Solid Surfaces, Interfaces and Thin Films*, pp. 100–103. Springer.

Mo, Y., Savage, D. E., Swartzentruber, B. S. & Lagally, M. G. (1990). *Phys. Rev. Lett.* **65**, 1020–1023.

Moorhead, M. S., Avedisian, C. T. & Kazimirov, A. Y. (2010). *10th AIAA/ASME Joint Thermophysics and Heat Transfer Conference*, Chicago, IL, USA.

Nguyen, T. D., Gronsky, R. & Kortricht, J. B. (1992). *MRS Proc.* **280**, 161.

Parratt, L. G. (1954). *Phys. Rev.* **95**, 359–369.

Pleshanov, N. K. (2004). *Nucl. Instrum. Methods Phys. Res. A*, **524**, 273–286.

Rutishauser, S., Rack, A., Weitkamp, T., Kayser, Y., David, C. & Macrander, A. T. (2013). *J. Synchrotron Rad.* **20**, 300–305.

Sawhney, K. J. S., Tiwari, M. K. & Alcock, S. G. (2011). *Proc. SPIE*, **8139**, 17–24.

Stampanoni, M., Groso, A., Isenegger, A., Mikuljan, G., Chen, Q., Bertrand, A., Henein, S., Betemps, R., Frommherz, U., Böhler, P., Meister, D., Lange, M. & Abela, R. (2006). *Proc. SPIE*, **6318**, 63180M.

Stearns, D. G. (1992). *J. Appl. Phys.* **71**, 4286–4298.

Störmer, M., Gabrisch, H., Horstmann, C., Heidorn, U., Hertlein, F., Wiesmann, J., Siewert, F. & Rack, A. (2016). *Rev. Sci. Instrum.* **87**, 051804.

Tu, Y., Zhu, J., Li, H., Jonnard, P., Le Guen, K., André, J., Chen, H. & Wang, Z. (2014). *Appl. Surf. Sci.* **313**, 341–345.

Walton, C. C. & Kortright, J. B. (1995). *Mater. Res. Soc. Symp.* **382**, 369–374.

Yumoto, H., Mimura, H., Matsuyama, S., Koyama, T., Hachisu, Y., Kimura, T., Yokoyama, H., Kim, J., Sano, Y., Tono, K., Togashi, T., Inubushi, Y., Sato, T., Tanaka, T., Yabashi, M., Ohashi, H., Ohmori, H., Ishikawa, T. & Yamauchi, K. (2013). *J. Phys. Conf. Ser.* **425**, 052022.

Zhang, L., Barrett, R., Friedrich, K., Glatzel, P., Mairs, T., Marion, P., Monaco, G., Morawe, C. & Weng, T. (2013). *J. Phys. Conf. Ser.* **425**, 052029.

Ziegler, E., Lepetre, Y., Joksch, S., Saile, V., Mourikis, S., Viccaro, P. J., Rolland, G. & Laugier, F. (1989). *Rev. Sci. Instrum.* **60**, 1999–2002.